A Microwave Imaging Approach based on Amplitude-only Data for the Reconstruction of the Electromagnetic Field Induced in Biological Phantoms

Salvatore Caorsi[1], Emanuela Bermani[2] and Andrea Massa[2]
[1]Dept. of Electronics, University of Pavia, Via Ferrata 1, I–27100 Pavia, Italy.
[2]DICA, University of Trento, via Mesiano 77, I–38050 Trento, Italy.

Abstract— **In this paper, a microwave imaging technique for the reconstruction of the electromagnetic field distribution inside exposed biological bodies from amplitude-only data is presented. The scattering problem, formulated in term of integral equations, is recast into an optimization problem after defining a suitable cost function which is proportional to the difference between reconstructed and measured amplitudes of the scattered and of the incident electric fields in the near-field region. The field solution is obtained by minimizing the cost function by means of an hybrid simulated annealing-conjugate gradient based procedure, which, in principle, ensures the convergence to the global minimum, preventing the solution from being trapped in local minima. Moreover, the proposed approach prevents the problems due to inaccuracies in near-field phase measurements. The effectiveness of the microwave imaging approach is assessed by means of some numerical examples (with synthetic input data) concerning a realistic cross-section of a biological phantom exposed to a TM electromagnetic illumination. The presence of noise on synthetic data is also considered and the dependence of the reconstruction accuracy on the signal-to-noise ratio investigated. Finally, in order to give some indications to further improve the prediction capability of the proposed approach, some preliminary guidelines are pointed out.**

Keywords— **Amplitude-only data, microwave imaging, electromagnetic field prediction, computational bioelectromagnetics.**

I. Introduction

In the last decade, the large diffusion of mobile communication systems and, consequently, the need to evaluate possible health risks has drawn great scientific and public attention to the study of the interaction between electromagnetic fields and biological bodies (see [1]-[3] and the references therein for a general overview).

Since a necessary first step for these research activities is represented by the prediction of the electromagnetic field distribution inside exposed biological bodies, a number of techniques, mainly based on the use of direct numerical methods, have been proposed [4]-[8]. Generally speaking, the problem addressed is the evaluation of the electromagnetic field induced in a reference phantom by an exactly known radiating source. Anatomically accurate biological models have been defined [9],[10] and various illumination conditions have been investigated by considering detailed numerical models of the electromagnetic sources [11], [12].

As far as inverse approaches are concerned, Caorsi and Massa proposed [13] and successively investigated [14] the effectiveness of an inverse scattering procedure based on a microwave imaging technique. Starting from an integral formulation of the scattering problem, the reconstruction of the electric field distribution is obtained by minimizing a suitable cost function. No modeling of the electromagnetic source is required. The input data for the minimization procedure are represented by the complex values of the incident field evaluated inside the investigation domain and of the scattered electric field measured outside the biological body during the electromagnetic exposure. Consequently, the approach seems to be suitable for in vivo evaluations. However, in real applications, while the measurement of the amplitude of the electric field does not represent a critical point, the evaluation of the phase distribution usually requires sophisticated equipment. Moreover, various factors make near-field phase measurements more and more inaccurate as the frequency increases. In more detail, errors in the probe position, temperature changes, mechanical movements of the cables connecting the probe to the receiver, variations in the relative humidity during the measurement and the stability and accuracy of the receiver strongly affect the accuracy of the measured near-field phase distribution. Moreover, the prohibitive cost of vector measurement apparatus can also be a substantial obstacle to obtaining phase information. Therefore, the development of a technique requiring only amplitude information is very attractive.

In the past, the use of phaseless data has already been proposed in the framework of near-field to far-field transformations [15] and antenna diagnostics [16]. Phase retrieval algorithms based on the measurement of the amplitude [17],[18] or of the squared amplitude

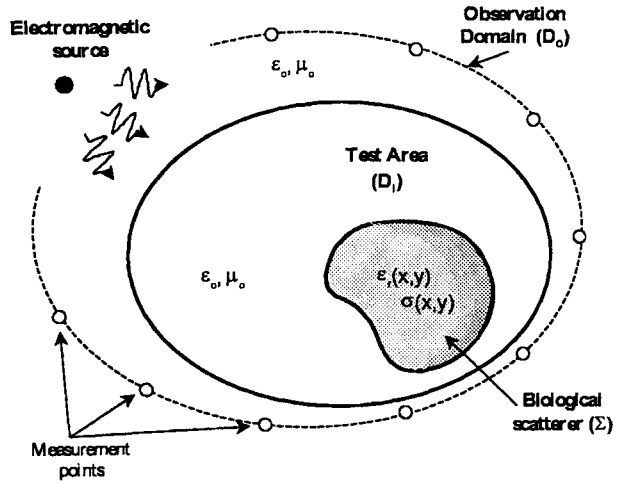

Fig. 1. Problem Geometry

[19] of the measured field have been investigated. However, to the best of authors' knowledge, no application of phaseless data techniques to electromagnetic field prediction in biological bodies has been proposed yet.

In the present work, the use of amplitude-only information for the prediction of the electromagnetic field distribution induced inside biological bodies is assessed in the framework of microwave imaging. The paper is organized as follows: in Section II, the microwave imaging approach is outlined, and the cost functional is defined. The differences with the approach proposed in [13] are outlined. Then, the minimization procedure is illustrated in Section III. Finally, some numerical simulations concerning the prediction of the electric field distribution inside a realistic cross-section of a biological phantom are reported and the robustness of the proposed hybrid technique to noisy data assessed.

II. Mathematical formulation

Let us consider a cylindrical biological object of arbitrary cross-section, Σ, characterized by known dielectric permittivity $\epsilon_r(x,y)$ and conductivity $\sigma(x,y)$, which belongs to a test area D_I. This object is illuminated by a TM-polarized wave whose electric field ϕ_i is parallel to the z-axis as depicted in Fig.1. The medium external to the object is assumed to be the vacuum characterized by a permittivity ϵ_0 and a permeability μ_0. Let ϕ represent the electric field and ϕ_s the diffracted field ($\phi_s = \phi - \phi_i$). According to the well-known electric field integral equation [21], the scattered field is given by

$$\phi_s(x,y) = \int_\Sigma G(x'y';x,y)\tau(x',y')\phi(x',y')dx'dy' \quad (1)$$

where k_0 is the wave number in the external medium, $\tau(x,y) = \epsilon_r(x,y) - 1 - j\frac{\sigma(x,y)}{2\pi f \epsilon_0}$, f is the frequency, and G is the two-dimensional Green's function of the external medium [21].

Moreover, the electric field satisfies the Lippmann-Schwinger integral equation [28]

$$\phi(x,y) - \int_\Sigma G(x'y';x,y)\tau(x',y')\phi(x',y')dx'dy' = = \phi_i(x,y) \quad (2)$$

Generally, in the inverse scattering approach for the field prediction the aim is to find the electric field distribution induced in an exposed biological body starting from the knowledge of both the amplitude and phase of the incident electric field and of the measured scattered electric field collected in an observation domain, D_o, external to the test area to which the scatterer belongs. Conversely, in the near-field phaseless approach only amplitude data are available. Then, different from the full-data approach presented in [13], we look for a field distribution that satisfies the following system

$$\Lambda_s(x,y) - - \left| \int_\Sigma G(x'y';x,y)\tau(x',y')\phi(x',y')dx'dy' \right| = 0 \quad (x,y) \in D_o$$

$$\Lambda_i(x,y) - - \left| \phi(x,y) - \int_\Sigma G(x'y';x,y)\tau(x',y')\phi(x',y')dx'dy' \right| = 0 \quad (x,y) \in \Sigma \quad (3)$$

where $\Lambda_s(x,y)$ and $\Lambda_i(x,y)$ represent the amplitudes of the scattered and incident fields, respectively.

In order to numerically solve this problem, system (3) is discretized according to the Richmond procedure [22]. To this end, we subdivide the investigation domain (i.e., the cross section of the biological model) into N square cells, where ϕ is approximated by a constant value, $\phi(x_n, y_n)$. Furthermore, Λ_s is collected at M points belonging to the observation domain (in the near field of the object). Then (3) can be rewritten as follows

$$\Lambda_s(\zeta_m,\xi_m) - - \left| \sum_{n=1}^{N} \{G(x_n,y_n;\zeta_m,\xi_m)\tau(x_n,y_n)\phi(x_n,y_n)\} \right| = 0 \quad m = 1,...,M$$

$$\Lambda_i(x_n,y_n) - |\phi(x_n,y_n) - \sum_{p=1}^{N} \{G(x_p,y_p;x_n,y_n)\tau(x_p,y_p)\phi(x_p,y_p)\} \Big| = 0 \quad n = 1,...,N \quad (4)$$

Due to unavoidable measurement errors and noise, the problem at hand is ill-posed, and it will be solved by considering the solution as the global minimum of the following cost function

$$\Omega\{\phi(x_n,y_n);n=1,...,N\} = \\ = \Omega_{Data}\{\phi(x_n,y_n);n=1,...,N\} + \\ + \Omega_{State}\{\phi(x_n,y_n);n=1,...,N\} \quad (5)$$

where

$$\Omega_{data}\{\phi(x_n,y_n);n=1...N\} = \\ = \frac{1}{\sum_{m=1}^{M}|\Lambda_s(\zeta_m,\xi_m)|^2}\cdot\sum_{m=1}^{M}\left|\Lambda_s(\zeta_m,\xi_m) - \right. \\ \left. - \left|\sum_{n=1}^{N}\{G(x_n,y_n;\zeta_m,\xi_m)\tau(x_n,y_n)\phi(x_n,y_n)\right|\right|^2 \quad (6)$$

$$\Omega_{State}\{\phi(x_n,y_n);n=1,...,N\} = \\ = \frac{1}{\sum_{n=1}^{N}|\Lambda_i(x_n,y_n)|^2}\cdot\sum_{n=1}^{N}\left|\Lambda_i(x_n,y_n) - \left|\phi(x_n,y_n) - \right.\right. \\ \left.\left. - \sum_{p=1}^{N}\{G(x_p,y_p;x_n,y_n)\tau(x_p,y_p)\phi(x_p,y_p)\}\right|\right|^2 \quad (7)$$

The non-quadratic nature of the functional to be minimized requires the use of an optimization technique able to avoid the convergence of the iterative solution on local minima.

III. Minimization procedure

Since the functional defined in (5) is non-quadratic with respect to the unknown array $\Phi = \{\phi(x_n,y_n); n=1,...,N\}$, it can exhibit local minima where deterministic algorithms can be trapped. In order to avoid the problem of *false* solutions which heavily effect the effectiveness of the field prediction procedure, an hybrid approach is proposed. Initially, a stochastic procedure based on the Metropolis criterion [14] is applied to initialize the search and to locate the *attraction basin* (i.e., the region around the global minimum). Once in this region, a Polak-Ribière conjugate gradient scheme [20] takes over to reach the optimum rapidly.

A. Simulated Annealing Procedure

In order to attain the *attraction basin*, we use an iterative procedure which is a modified version of the simulated annealing approach [23] (MSA). In the past, it has been proven that simulated annealing can be successfully applied to the solution of electromagnetic inverse scattering problems [24], [25] as well as for nonlinear direct scattering problems [26] where the problem of false solutions arises. The great power of the approach lies first in its flexibility which allows the cost function to be simple or complicated and permits efficient treatment of a large number of unknowns. Moreover, it allows all the available *a-priori knowledge* about the physical model of the unknowns to be taken into account. Even though the solution must be randomly chosen at each iteration, the range of possible values can be suitably restricted (when selecting the solution at each iteration) to only those values that are physically appropriate. This fact restricts the random search from the whole space of unknowns to a limited subspace, simplifying the search for the *attraction basin.*

In more detail, MSA starts from an initial estimate of the field distribution $\Phi^{(0)} = \{\phi^{(0)}(x_n,y_n); n=1,...,N\}$ and fix a control parameter, T_0 (i.e., the "temperature of the system"), which is slowly decreased during the iterative process.

Starting from the initial state, the algorithm tries to locate the *attraction basin* by generating a sequence of values to be assigned to the unknown array, $\Phi^{(k)}$, according to the *raster rule* [14]. For each nth subdomain, the value of the estimated field at the kth iteration is changed as follows

$$\phi_t^{(k)}(x_n,y_n) = \\ = \begin{cases} (\eta+1)\phi^{(k)}(x_n,y_n) & \textit{with probability } P_0 \\ \sum_{\ell=1}^{L}\phi^{(k)}(x_\ell,y_\ell) & \textit{with probability } (1-P_0) \end{cases} \quad (8)$$

where L is the dimension of the neighborhood set of the current subdomain, and η is a value randomly chosen in the range between -1 and 1.

Changes are driven by the Metropolis criterion. If the new array $\Phi^t = \{\phi^{(k)}(x_1,y_1),\ldots,\phi^{(k)}(x_{n-1},y_{n-1}), \phi_t^{(k)}(x_n,y_n), \phi^{(k)}(x_{n+1},y_{n+1}),\ldots,\phi^{(k)}(x_N,y_N)\}$ causes the system be in a lower-energy state, the new value is unconditionally accepted, otherwise the new distribution is accepted with probability $p = exp\left\{-\frac{\Omega\{\Phi^t\}-\Omega\{\Phi^{(k)}\}}{T_k}\right\}$, or rejected with probability $(1-p)$. Once the scanning of the N investigation subdomains is completed, the estimated electric field configuration is kept for the next iteration ($\phi^{(k+1)} \leftarrow \phi_t^{(k)}$) and the temperature is updated according to a logarithmic scheduling

$$T_{k+1} = \frac{T_0}{ln(1+k)} \quad (9)$$

which ensures the convergence of the iterative approach [27].

The iterative procedure is repeated until the threshold for the stopping criterion is reached ($\Omega\left\{\Phi^{(k_{opt})}\right\} \leq \gamma_{th}$), or when the iterative loop is completed ($k = K_{max}$), or until a given criterion for switching the MSA to the gradient-based algorithm is attained.

B. Switch Criterion

The criterion for stopping the MSA and switching to the CG algorithm is satisfied when the following conditions hold:

1. *stationary condition*

$$\frac{\left|K_{window}\Omega_{opt}^{(k)} - \sum_{i=1}^{K_{window}} \Omega_{opt}^{(i)}\right|}{\Omega_{opt}^{(i)}} \leq \gamma_{st},\ k = K_{switch} \tag{10}$$

where $\Omega_{opt}^{(k)} = min_{i=0,\ldots,k}\left\{\Omega\left\{\Phi^{(i)}\right\}\right\}$, K_{window} is a fixed number of iterations, γ_{st} is an assigned threshold, and

2. *slope condition*

$$\left|\nabla\Omega_{opt}^{(K_{switch})}\right| \geq \gamma_{th} \tag{11}$$

where $\nabla\Omega$ is the gradient vector, whose q*th* component is defined as

$$(\nabla\Omega)_q = \left\{\frac{\partial\Omega}{\partial Re\left\{\phi\left(x_q, y_q\right)\right\}}\right\} + j\left\{\frac{\partial\Omega}{\partial Im\left\{\phi\left(x_q, y_q\right)\right\}}\right\} \tag{12}$$

The evaluation of $\nabla\Omega$ is detailed in Appendix A.

C. Conjugate Gradient Procedure

Since the main drawback of the MSA is the low convergence rate to the global optimum when the attraction basin is attained, in order to increase the convergence speed of the algorithm an iterative procedure based on Polak-Ribière method [20] is applied.

Let us now summarize the steps of the applied deterministic technique.

1. Set the initial guess of the deterministic procedure equal to the best solution obtained at the switch iteration

$$\Phi^{(k_{GC})} = \Phi_{opt}^{(K_{switch})} \qquad k_{GC} = 1 \tag{13}$$

where k_{GC} indicates the iteration number during the deterministic procedure.

2. Compute the direction vector

$$d^{(k_{GC})} = -\nabla\Omega\left\{\Phi_{opt}^{(K_{switch})}\right\} \qquad k_{GC} = 1 \tag{14}$$

3. Find the optimal step $\nu^{(k_{GC})}$ ensuring the maximum decrease of Ω along the updating direction, which minimizes the function $\Omega\left\{\Phi^{(k_{GC})} + \nu^{(k_{GC})}d^{(k_{GC})}\right\}$

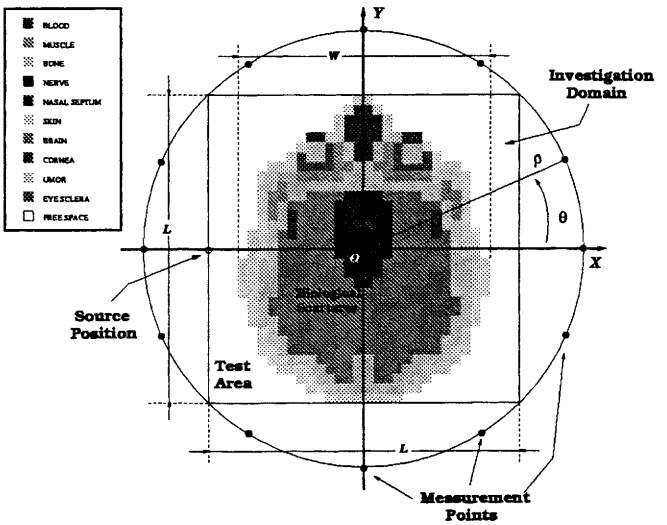

Fig. 2. Model of the biological scatterer

4. Compute the new solution

$$\Phi^{(k_{GC}+1)} = \Phi^{(k_{GC})} + \nu^{(k_{GC})}d^{(k_{GC})} \tag{15}$$

5. If the convergence threshold is reached (i.e., $\Omega\left\{\Phi^{(k_{GC}+1)}\right\} \leq \gamma_{th}$) then stop the iterative process, and regard the current solution as the estimated electric field distribution inside the biological body. Otherwise compute the new direction vector as follows

$$d^{(k_{GC}+1)} = -\nabla\Omega\left\{\Phi^{(k_{GC}+1)}\right\} + \beta^{(k_{GC}+1)}d^{(k_{GC})} \tag{16a}$$

$$\beta^{(k_{GC}+1)} = max\left\{\frac{\left[\nabla\Omega\left\{\Phi^{(k_{GC}+1)}\right\}\right]^T}{\left[\nabla\Omega\left\{\Phi^{(k_{GC})}\right\}\right]^T\left[\nabla\Omega\left\{\Phi^{(k_{GC})}\right\}\right]}\cdot\left[\nabla\Omega\left\{\Phi^{(k_{GC}+1)}\right\} - \nabla\Omega\left\{\Phi^{(k_{GC})}\right\}\right], 0\right\} \tag{16b}$$

and return to step 3.

IV. Numerical Results

In order to test the effectiveness of the proposed approach, we performed some numerical simulations, with data synthetically obtained, concerning the reconstruction of the electric field distribution inside the cross-section of a known biological phantom placed in vacuum. Figure 2 shows the configuration considered. The dielectric parameters are reported in Table I [29].

The cross-section of the biological scatterer, located at the center of a square test area $l = 0.581\lambda_0$-sided (where λ_0 is the free-space wavelength), is subdivided into 598 square cells. Thirty-two measurement points

TABLE I
ELECTRICAL PROPERTIES OF THE TISSUES IN THE CROSS-SECTION OF THE BIOLOGICAL PHANTOM

	ϵ_r	σ(S/m)
Blood	61.36	1.5379
Bone	12.454	$1.4331 \cdot 10^{-1}$
Brain	52.725	$9.4227 \cdot 10^{-1}$
Cornea	55.235	1.3943
Eye-sclera	55.271	1.1668
Muscle	55.032	$9.4294 \cdot 10^{-1}$
Nasal-septum	42.635	$7.8239 \cdot 10^{-1}$
Nerve	32.531	$5.7369 \cdot 10^{-1}$
Skin	41.405	$8.6674 \cdot 10^{-1}$
Umor	68.902	1.6362

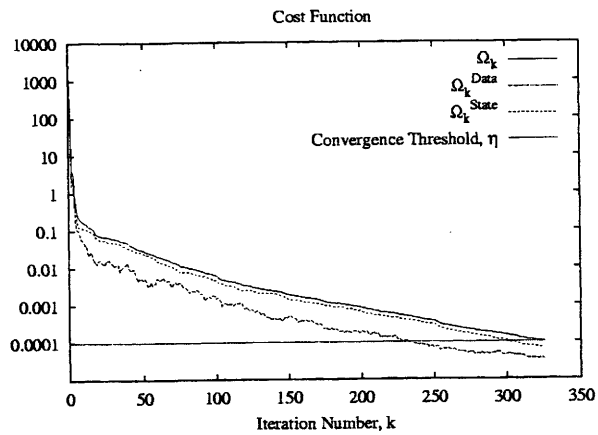

Fig. 3. Conjugate gradient procedure. Behaviour of the fitness function versus the number of iteration

are placed on a circle $\rho = 0.451\lambda_0$ in radius, belonging to the observation domain. In order to avoid the possibility that errors in the forward and inverse solutions tend to cancel, the data for the inversion procedure (i.e, the values of the scattered electric field at the measurement points) are computed by means of the Richmond procedure with a different discretization of the scatterer under test ($\Delta q_{Direct} = \frac{\Delta q}{2}$, $\Delta q = 0.018\lambda_0$).

The electromagnetic source is an infinite electric line of current placed near the biological scatterer in the horizontal axis at a distance $a = 0.288\lambda_0$ from the center of the reference coordinate system.

For this source, the radiated field is given by

$$\phi_i(x,y) = -I\frac{k_0^2}{8\pi f\varepsilon_0}H_0^{(2)}(k_0 r) \qquad (17)$$

where $H_0^{(2)}$ is the Hankel function of the second kind and $0th$ order, and r is the distance between the source and a point (x,y). The value of I is chosen so that a

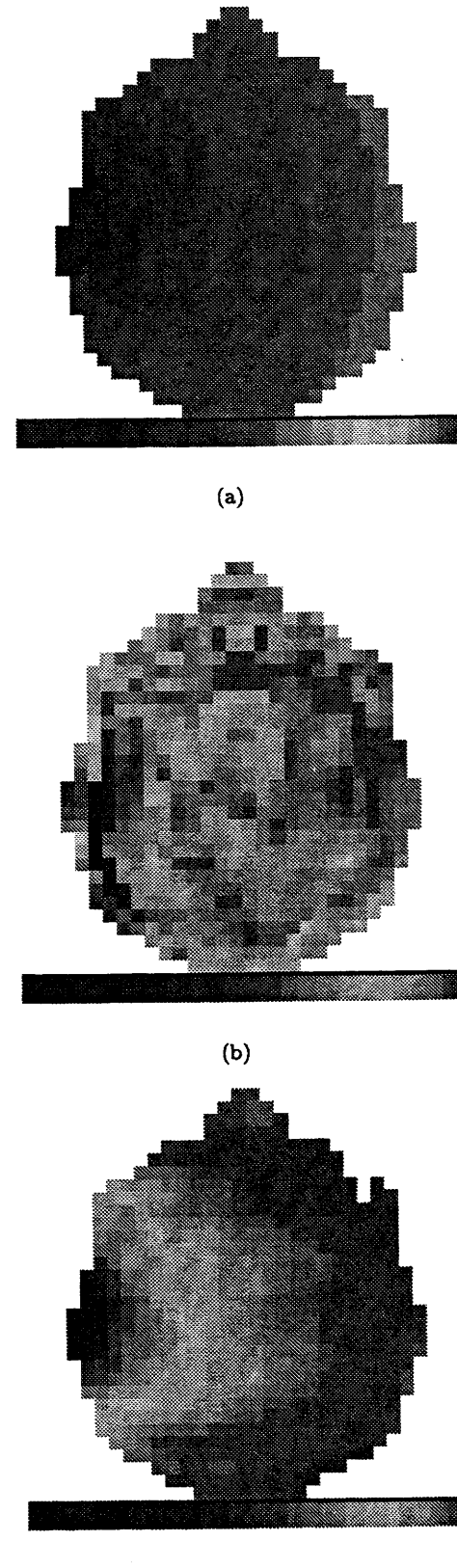

Fig. 4. Conjugate gradient procedure. Images of the electric field amplitude: (a) intial guess ($k = 0$), (b) result at the convergence iteration ($k = k_{opt}$) and (c) actual distribution.

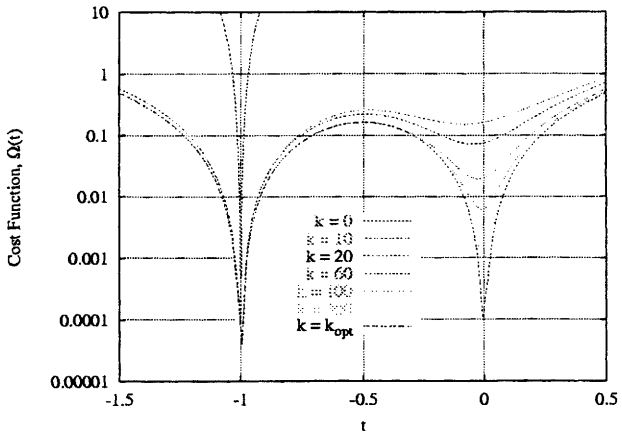

Fig. 5. Coniugate gradient procedure. Behaviour of the functional $\Omega(t)$ along the direction defined by the parametric equation $f(t) = (1+t)\phi^k - t\phi_{actual}$

radiated power per unit length of $P = 0.25mW/meter$ is generated.

As a first result, we will show that when a deterministic procedure is applied to minimize the functional (5), the computed solution could be trapped in a local minimum if the initial distribution is not properly chosen. To this end, let us consider the conjugate-gradient method as the minimization algorithm, and let us assume the initial electric field distribution equal to that of the incident field (Fig. 4(a)). Figure 3 shows that, even if, at the stopping iteration, the cost function value is less than the convergence threshold ($\gamma_{th} = 10^{-4}$), the amplitude of the electric fields inside the biological scatterer is not reconstructed with sufficient accuracy, as can be seen comparing the actual distribution (Fig. 4(c)) with the predicted one (Fig. 4(b)). This is due to the presence of undesired local minima where the algorithm is trapped. Since we are dealing with synthetic data, it is possible to state that the conjugate-gradient procedure (and, more generally, deterministic procedures) could lead to false solutions corresponding to local minima of the functional.

Figure 5 shows the plot of Ω along a direction in the solution space joining the actual solution Φ_{actual} to the solution at different iterations of the iterative process $\Phi^{(k)}$ whose parametric equation is given by

$$f(t) = (1+t)\Phi^{(k)} - t\Phi_{actual} \qquad (18)$$

The plot clearly points out that the solution attained when the iterative procedure is stopped, $\Phi^{(k_{opt})}$, is not the global minimum of the functional.

In order to overcome this problem and to enhance the reconstruction quality, the hybrid optimization approach is used.

Figure 6 gives some indications about the behavior of the functional to be minimized along the direction

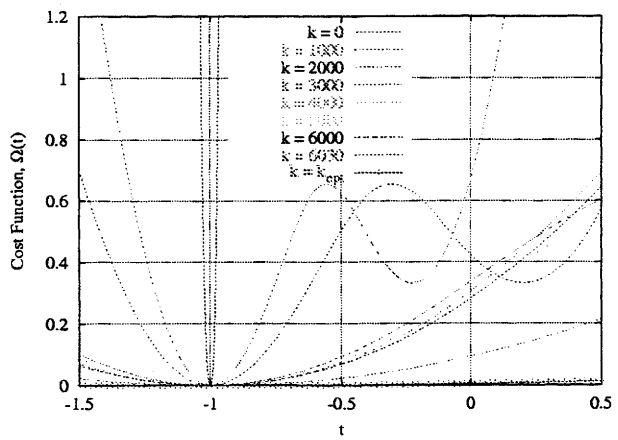

(a)

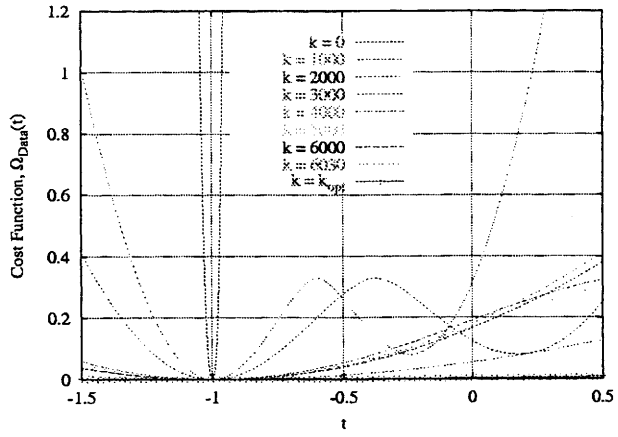

(b)

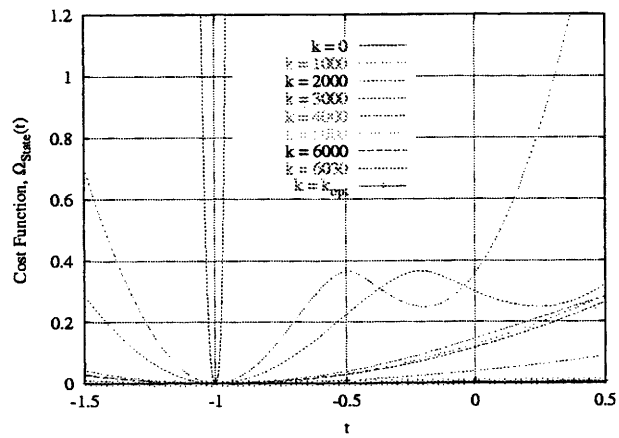

(c)

Fig. 6. Hybrid procedure. Behaviour of the functionals (a) $\Omega(t)$, (b) $\Omega_{data}(t)$, and (c) $\Omega_{state}(t)$ along the direction defined by the parametric equation $f(t) = (1+t)\phi^{(k)} - t\phi_{actual}$

given by equation (18). In particular, Figs. 6(a), 6(b) and 6(c) show the plots of the cost function, of the data term and of the state term in correspondence with the solutions estimated at different iterations, respectively. Clearly, the plots relating to the iterations $k = 1000$ and $k = 2000$ show the presence of local minima in the cost function which are avoided by the hybrid procedure as confirmed from the plots of the successive iterations. The value of the cost function reached at the iteration k_{opt} is very close to that of the global minimum.

Consequently, a notable improvement in the field reconstruction is obtained when the hybrid approach is applied. Figure 7 gives the color-level images of the reconstructed field distribution at different iterations. The plots show that starting from the iteration $k = 5000$ (Fig. 7(c)), the field distribution becomes more and more similar to the reference solution (Fig. 4(c)) and also the amplitude values are more and more close to the actual ones. The above considerations are confirmed by the statistics of the error figure $\xi(x, y)$, defined as

$$\xi(x,y) = \frac{||\phi(x,y)| - |\phi_{actual}(x,y)||}{max_{(x,y)}\{|\phi_{actual}(x,y)|\}} \quad (x,y) \in \Sigma \tag{19}$$

where $\phi_{actual}(x, y)$ are the actual field values at points inside the biological scatterer, which are given in Table II. The statistics for the full-data reconstruction procedure are also reported. Finally, we can also observe that the location and the order of magnitude of the absorption peak (of fundamental importance in order to give some indications about the power levels induced inside the biological body for safety evaluations) are correctly evaluated at the convergence iteration (the location error is less than the size of the discretization cell, and the difference between the reconstructed and reference amplitudes is less than 10%. For completeness, Figure 8 shows the plot of the cost function as a function of the number of iterations for one optimization run, corresponding to the prediction results reported in Figure 7. In this case, the parameters assumed for the proposed hybrid algorithm are the following: $T_0 = \frac{\sum_{m=1}^{M}|\Lambda_s(x_m,y_m)|^2}{N}$, $K_{max} = 10000$, $K_{window} = 0.1K_{max}$ and $\gamma_{st} = 10^{-3}$. Also the values of the data (Ω_{Data}) and of the state (Ω_{State}) terms are reported. During the inversion procedure, these quantities give an idea of the fit with the input data. The *state term* and the *data term* check whether the trial solution satisfies the equation describing the scattering phenomena inside and outside the biological scatterer, respectively. The graphs related to these terms show damped oscillatory behaviors, which are specific for the algorithm used to reach the convergence, whereas the plot of Ω is always decreasing because it reports the minimum value reached until the current iteration.

TABLE II
HYBRID PROCEDURE. STATISTICS OF THE ERROR FIGURE ξ FOR DIFFERENT NUMBER OF ITERATIONS

	k	min{ξ}	max{ξ}	av{ξ}	var{ξ}
Phase-less Data	0	$8.94\cdot10^{-1}$	1.524	1.131	0.016
	1000	$7.19\cdot10^{-3}$	4.973	1.355	1.136
	3000	$1.45\cdot10^{-3}$	1.182	0.280	0.064
	5000	$1.19\cdot10^{-3}$	1.091	0.257	0.054
	6000	$2.84\cdot10^{-4}$	1.036	0.261	0.053
	6030	$1.0\cdot10^{-4}$	0.602	0.144	0.017
	k^*	$1.67\cdot10^{-4}$	0.248	0.095	0.009
Full Data	k^*	$1.48\cdot10^{-7}$	0.0009	0.0001	$2.7\cdot10^{-6}$

Finally, as the noise is a significant problem in practical applications, the effectiveness of the prediction process, when an additive noise is present, has been preliminarily analyzed. In more detail, for the same configuration, we considered the influence of a Gaussian noise simulated by adding to the data a complex value in which the real and imaginary parts are Gaussian variables, characterized by zero mean value and by a variance that can be obtained in a straightforward way once the value of the signal-to-noise ratio (SNR) has been fixed. Table III gives the statistics of the error figure for different values of SNR. Referring to the mean values, it can be noted that the prediction error increases as SNR decreases. Nevertheless, the reconstruction quality can be considered acceptable (percentage errors smaller than 30%) for $SNR \geq 20dB$. As expected, notable errors are encountered for the lowest values of the signal-to-noise ratio. However, it must be pointed out that a more sophisticated noise model is necessary in order to accurately simulate realistic situations.

TABLE III
HYBRID PROCEDURE. STATISTICS OF THE ERROR FIGURE ξ FOR DIFFERENT VALUES OF THE SIGNAL-TO-NOISE RATIO

SNR(dB)	min{ξ}	max{ξ}	av{ξ}	var{ξ}
50	$7.99\cdot10^{-6}$	1.032	0.177	0.041
40	$1.93\cdot10^{-4}$	1.027	0.233	0.053
30	$1.60\cdot10^{-5}$	1.042	0.241	0.054
20	$1.84\cdot10^{-4}$	0.929	0.258	0.055
10	$2.07\cdot10^{-3}$	2.164	0.386	0.082
5	$3.42\cdot10^{-3}$	1.875	0.506	0.118

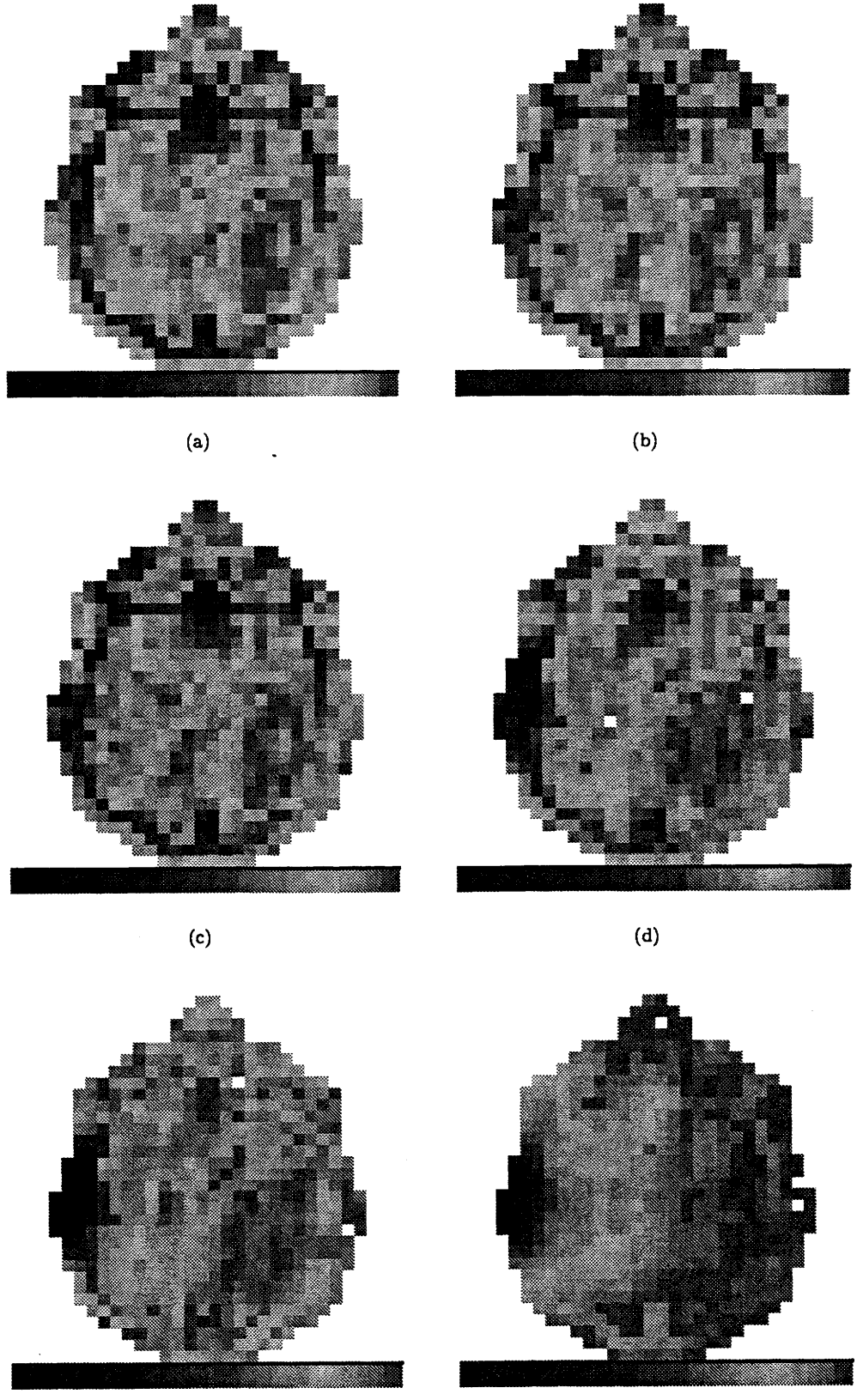

Fig. 7. Hybrid procedure. Images of the electric field amplitude. Estimated amplitude at the iterations (*a*) $k = 1000$, (*b*) $k = 3000$, (*c*) $k = 5000$, (*d*) $k = 6000$, (*e*) $k = 6030$, and (*f*) $k = k_{opt}$.

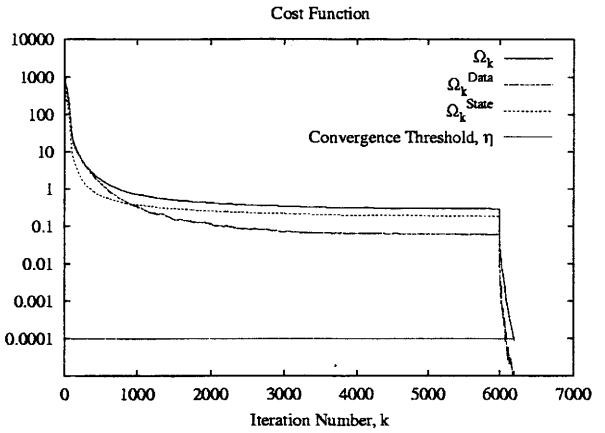

Fig. 8. Hybrid procedure. Behaviour of the fitness function versus the number of iterations

V. Conclusions

The problem of the prediction of the electric field distribution inside biological phantoms starting from amplitude-only data has been addressed for two-dimensional geometries. An approach based on a hybrid stochastic/deterministic iterative procedure has been presented, described and discussed throughout this paper. The algorithm has been applied to reach the minimum of a suitably defined cost function without the solution being trapped in local minima which typically arise in nonlinear inverse problems.

Numerical results have been reported for a cross-section of a realistic biological scatterer inside a region under test illuminated by a TM incident electric field. It has been possible to reconstruct the induced field distribution even on the basis of measurement data affected by Gaussian noise. Results prove the possibility of attaining qualitative indications about the amplitude distribution as well as the location of the amplitude peak. The results are preliminary but promising. What is more, the capabilities of the present approach could be increased by adding linear constraints on the field distribution in order to obtain a reduction of independent unknowns, limiting the search space and simplifying the solution of the problem.

VI. Appendix A

In this appendix the expression for the vector $\nabla\Omega$ given by

$$\nabla\Omega = \nabla\Omega_{Data} + \nabla\Omega_{State} \tag{A.1}$$

is derived. The computation of the partial derivatives of Ω_{Data} and of Ω_{State} with respect to the variables $Re\{\phi(x_q,y_q)\}$ and $Im\{\phi(x_q,y_q)\}$ $q = 1,...,N$ is required (where $Re\{\}$ and $Im\{\}$ indicate the real and imaginary parts, respectively).

First of all, let us give some preliminary definitions

$$\Im_m^{Data} = \Lambda_s(\zeta_m,\xi_m) - \left|\phi_s^{(rec)}(\zeta_m,\xi_m)\right| \tag{A.2}$$

$$\Im_n^{State} = \left|\phi_i^{(rec)}(x_n,y_n)\right| - \Lambda_i(x_n,y_n) \tag{A.3}$$

where $\phi_s^{(rec)}(\zeta_m,\xi_m) = k_0^2\sum_{n=1}^{N}\{G(x_n,y_n;\zeta_m,\xi_m)\cdot\tau(x_n,y_n)\phi(x_n,y_n)\}$ and $\phi_i^{(rec)}(x_m,y_m) = \phi(x_n,y_n) - -k_0^2\sum_{p=1}^{N}\{G(x_p,y_p;x_n,y_n)\tau(x_p,y_p)\phi(x_p,y_p)\}$.

As far as the data-term is concerned, it is useful to evaluate the partial derivatives of $\Im_m^{Data}$. By means of simple mathematical manipulations, the following expression are obtained

$$\frac{\partial\Im_m^{Data}}{\partial Re\{\phi(x_q,y_q)\}} = -\frac{1}{\left|\phi_s^{(rec)}(\zeta_m,\xi_m)\right|}\cdot \left\{Re\left\{\phi_s^{(rec)}(\zeta_m,\xi_m)\right\}\frac{\partial Re\left\{\phi_s^{(rec)}(\zeta_m,\xi_m)\right\}}{\partial Re\{\phi(x_q,y_q)\}} + Im\left\{\phi_s^{(rec)}(\zeta_m,\xi_m)\right\}\frac{\partial Im\left\{\phi_s^{(rec)}(\zeta_m,\xi_m)\right\}}{\partial Re\{\phi(x_q,y_q)\}}\right\} \tag{A.4}$$

$$\frac{\partial\Im_m^{Data}}{\partial Im\{\phi(x_q,y_q)\}} = -\frac{1}{\left|\phi_s^{(rec)}(\zeta_m,\xi_m)\right|}\cdot \left\{Re\left\{\phi_s^{(rec)}(\zeta_m,\xi_m)\right\}\frac{\partial Re\left\{\phi_s^{(rec)}(\zeta_m,\xi_m)\right\}}{\partial Im\{\phi(x_q,y_q)\}} + Im\left\{\phi_s^{(rec)}(\zeta_m,\xi_m)\right\}\frac{\partial Im\left\{\phi_s^{(rec)}(\zeta_m,\xi_m)\right\}}{\partial Im\{\phi(x_q,y_q)\}}\right\} \tag{A.5}$$

where

$$\frac{\partial Re\left\{\phi_s^{(rec)}(\zeta_m,\xi_m)\right\}}{\partial Re\{\phi(x_q,y_q)\}} = -\frac{\pi k_0\Delta q}{2}\{\varepsilon_r(x_q,y_q)-1\}J_1(k_0\Delta q)Y_0(k_0\rho_{mq}) - -\frac{\pi k_0\Delta q\sigma(x_q,y_q)}{4\pi f\varepsilon_0}J_1(k_0\Delta q)J_0(k_0\rho_{mq}) \tag{A.6}$$

$$\frac{\partial Re\left\{\phi_s^{(rec)}(\zeta_m,\xi_m)\right\}}{\partial Im\{\phi(x_q,y_q)\}} = -\frac{\pi k_0\Delta q\sigma(x_q,y_q)}{4\pi f\varepsilon_0}J_1(k_0\Delta q)Y_0(k_0\rho_{mq}) + +\frac{\pi k_0\Delta q}{2}\{\varepsilon_r(x_q,y_q)-1\}J_1(k_0\Delta q)J_0(k_0\rho_{mq}) \tag{A.7}$$

$$\frac{\partial Im\left\{\phi_s^{(rec)}(\zeta_m,\xi_m)\right\}}{\partial Re\{\phi(x_q,y_q)\}} = \\ = -\frac{\pi k_0 \Delta q}{2}\left\{\varepsilon_r(x_q,y_q)-1\right\} J_1(k_0\Delta q)\, J_0(k_0\rho_{mq}) + \\ + \frac{\pi k_0 \Delta q \sigma(x_q,y_q)}{4\pi f \varepsilon_0} J_1(k_0\Delta q)\, Y_0(k_0\rho_{mq}) \tag{A.8}$$

$$\frac{\partial Im\left\{\phi_s^{(rec)}(\zeta_m,\xi_m)\right\}}{\partial Im\{\phi(x_q,y_q)\}} = \frac{\partial Re\left\{\phi_s^{(rec)}(\zeta_m,\xi_m)\right\}}{\partial Re\{\phi(x_q,y_q)\}} \tag{A.9}$$

where $\Delta q = \sqrt{\frac{A_q}{\pi}}$, and A_q is the area of the q*th* discretization cell.

Accordingly, the partial derivatives of Ω_{Data} with respect to $Re\{\phi(x_q,y_q)\}$ and $Im\{\phi(x_q,y_q)\}$ given by

$$\frac{\partial \Omega_{Data}}{\partial Re\{\phi(x_q,y_q)\}} = \frac{2\sum_{m=1}^{M}\left\{\Im_m^{Data}\frac{\partial \Im_m^{Data}}{\partial Re\{\phi(x_q,y_q)\}}\right\}}{\sum_{m=1}^{M}\left|\Lambda_s(\zeta_m,\xi_m)\right|^2} \tag{A.10}$$

$$\frac{\partial \Omega_{Data}}{\partial Im\{\phi(x_q,y_q)\}} = \frac{2\sum_{m=1}^{M}\left\{\Im_m^{Data}\frac{\partial \Im_m^{Data}}{\partial Im\{\phi(x_q,y_q)\}}\right\}}{\sum_{m=1}^{M}\left|\Lambda_s(\zeta_m,\xi_m)\right|^2} \tag{A.11}$$

are evaluated as

$$\frac{\partial \Omega_{Data}}{\partial Re\{\phi(x_q,y_q)\}} = \frac{\pi k_0 \Delta q J_1(k_0\Delta q)}{\sum_{m=1}^{M}|\Lambda_s(\zeta_m,\xi_m)|^2}\cdot \\ \sum_{m=1}^{M}\left\{\frac{\Lambda_s(\zeta_m,\xi_m)}{\left|\phi_s^{(rec)}(\zeta_m,\xi_m)\right|}-1\right\}\left\{Re\left\{\phi_s^{(rec)}(\zeta_m,\xi_m)\right\}\cdot\right. \\ \left\{\left\{\varepsilon_r(x_q,y_q)-1\right\}Y_0(k_0\rho_{mq}) + \frac{\sigma(x_q,y_q)}{2\pi f\varepsilon_0}J_0(k_0\rho_{mq})\right\} + \\ + \left\{\left\{\varepsilon_r(x_q,y_q)-1\right\}J_0(k_0\rho_{mq}) - \frac{\sigma(x_q,y_q)}{2\pi f\varepsilon_0}Y_0(k_0\rho_{mq})\right\}\cdot \\ \left.Im\left\{\phi_s^{(rec)}(\zeta_m,\xi_m)\right\}\right\} \tag{A.12}$$

$$\frac{\partial \Omega_{Data}}{\partial Im\{\phi(x_q,y_q)\}} = \frac{\pi k_0 \Delta q J_1(k_0\Delta q)}{\sum_{m=1}^{M}|\Lambda_s(\zeta_m,\xi_m)|^2}\cdot \\ \sum_{m=1}^{M}\left\{\frac{\Lambda_s(\zeta_m,\xi_m)}{\left|\phi_s^{(rec)}(\zeta_m,\xi_m)\right|}-1\right\}\left\{Im\left\{\phi_s^{(rec)}(\zeta_m,\xi_m)\right\}\cdot\right. \\ \left\{\frac{\sigma(x_q,y_q)}{2\pi f\varepsilon_0}J_0(k_0\rho_{mq}) - \frac{2\{\varepsilon_r(x_q,y_q)-1\}}{\pi k_0\Delta q}Y_0(k_0\rho_{mq})\right\} - \\ - \left\{\left\{\varepsilon_r(x_q,y_q)-1\right\}J_0(k_0\rho_{mq}) - \frac{\sigma(x_q,y_q)}{2\pi f\varepsilon_0}Y_0(k_0\rho_{mq})\right\}\cdot \\ \left.Re\left\{\phi_s^{(rec)}(\zeta_m,\xi_m)\right\}\right\} \tag{A.13}$$

Analogously, it is possible to evaluate the partial derivatives of Ω_{State}, which are given by

$$\frac{\partial \Omega_{State}}{\partial Re\{\phi(x_q,y_q)\}} = \frac{\pi k_0 \Delta q}{\sum_{n=1}^{N}|\Lambda_i(x_n,y_n)|^2}\cdot \\ \sum_{n=1}^{N}\left\{1-\frac{\Lambda_i(x_n,y_n)}{\left|\phi_i^{(rec)}(x_n,y_n)\right|}\right\}\left\{Re\left\{\phi_i^{(rec)}(x_n,y_n)\right\}\cdot\right. \\ \left\{\frac{2}{\pi k_0\Delta q}\delta_{nq} + \left\{\varepsilon_r(x_q,y_q)-1\right\}\Lambda_{nq} + \frac{\sigma(x_q,y_q)}{2\pi f\varepsilon_0}\Pi_{nq}\right\} - \\ - \left\{\frac{\sigma(x_q,y_q)}{2\pi f\varepsilon_0}\Lambda_{nq} - \left\{\varepsilon_r(x_q,y_q)-1\right\}\Pi_{nq}\right\}\cdot \\ \left.Im\left\{\phi_i^{(rec)}(x_n,y_n)\right\}\right\} \tag{A.14}$$

$$\frac{\partial \Omega_{State}}{\partial Im\{\phi(x_q,y_q)\}} = \frac{\pi k_0 \Delta q}{\sum_{n=1}^{N}|\Lambda_i(x_n,y_n)|^2}\cdot \\ \sum_{n=1}^{N}\left\{1-\frac{\Lambda_i(x_n,y_n)}{\left|\phi_i^{(rec)}(x_n,y_n)\right|}\right\}\left\{Re\left\{\phi_i^{(rec)}(x_n,y_n)\right\}\cdot\right. \\ \left\{\frac{\sigma(x_q,y_q)}{2\pi f\varepsilon_0}\Lambda_{nq} - \left\{\varepsilon_r(x_q,y_q)-1\right\}\Pi_{nq}\right\} + \\ + \left\{\frac{2}{\pi k_0\Delta q}\delta_{nq} + \left\{\varepsilon_r(x_q,y_q)-1\right\}\Lambda_{nq} + \frac{\sigma(x_q,y_q)}{2\pi f\varepsilon_0}\Pi_{nq}\right\}\cdot \\ \left.Im\left\{\phi_i^{(rec)}(x_n,y_n)\right\}\right\} \tag{A.15}$$

where

$$\Lambda_{nq} = \begin{cases} Y_1(k_0\Delta q) + \frac{2}{\pi k_0\Delta q} & n=q \\ J_1(k_0\Delta q)\, Y_0(k_0\rho_{qn}) & n\neq q \end{cases} \tag{A.16}$$

$$\Pi_{nq} = \begin{cases} 1 & n=q \\ J_0(k_0\rho_{qn}) & n\neq q \end{cases} \tag{A.17}$$

and $\delta_{nq}=1$ if $n=q$, $\delta_{nq}=0$ otherwise.

Finally, the array $\nabla\Omega = \{(\nabla\Omega)_q; q=1,...,N\}$ can be computed as

$$(\nabla\Omega)_q = \left\{\frac{\partial \Omega_{State}}{\partial Re\{\phi(x_q,y_q)\}} + \frac{\partial \Omega_{Data}}{\partial Re\{\phi(x_q,y_q)\}}\right\} + \\ + \quad j\left\{\frac{\partial \Omega_{State}}{\partial Im\{\phi(x_q,y_q)\}} + \frac{\partial \Omega_{Data}}{\partial Im\{\phi(x_q,y_q)\}}\right\} \tag{A.18}$$

REFERENCES

[1] M. A. Stuchly, "Wireless communications and the safety of the user," *Journal of Wireless Information Networks*, vol. 1, no. 4, pp. 223-228, Oct. 1994.

[2] M. A. Stuchly, "Mobile communication systems and biological effects on their users," *Radio Science Bulletin*, no. 275, pp. 7-13, Dec. 1995.

[3] M. A. Stuchly, "Biomedical concerns in wireless communications," *Critical Reviews in Biomedical Engineering*, vol. 26, no. 1-2, pp.117-151, 1998.

[4] J. C. Lin and O. P. Gandhi, "Computational method for predicting field intensity," in *Handbook of Biological Effects of Electromagnetic Fields*, C. Polk and E. Postow, Eds. Boca Raton, FL: CRC Press, pp. 337-402, 1995.

[5] K. Caputa, M. Okoniewski, and M. A. Stuchly, "An algorithm for computations of the power deposition in human

tissue," *IEEE Antennas Propagat. Magaz.*, vol. 41, no. 4, pp. 102-107, Aug. 1999.

[6] U. Jakobus, F. M. Landstorfer, "Current-based hybrid moment method analysis of electromagnetic radiation and scattering problems," *ACES Journal*, vol. 10, no. 3, pp. 38-46, Nov. 1995.

[7] H. O. Ruoss, U. Jakobus, F. M. Landstorfer, "Efficient EM analysis of hand-held mobile telephones close to human head using modified method of moments," *Electronics Letters*, vol. 31, no. 12, pp. 947-948, June 1995.

[8] D. M. Sullivan, O. P. Gandhi, and A. Taflove, "Use of the finite-difference time-domain method for calculating EM absorption in man models," *IEEE Trans. Biomed. Eng.*, vol. 35, pp. 179-186, Mar. 1988.

[9] G. Lazzi, and O. P. Gandhi, "Realistically Tilted and Truncated Anatomically Based Models of the Human Head for Dosimetry of Mobile Telephones," *IEEE Transactions on Electromagnetic Compatibility*, vol. 39, pp. 55-61, Feb. 1997.

[10] A. D. Tinniswood, C. M. Furse and O. P. Gandhi, "Computation of SAR distributions for two anatomically based models of the human head using CAD files of commercial telephones and the parallelized FDTD code," *IEEE Trans. Antennas Propagat.*, vol. 46, pp. 829-833, June 1998.

[11] G. Lazzi and O. P. Gandhi, "On modeling and personal dosimetry of normal mode helical antennas with the FDTD code," *IEEE Antennas Propagat.*, vol. 46, pp. 525-530, Apr. 1998.

[12] M. Okoniewski, M. Ali, M. Douglas, M. A. Stuchly, and S. S. Stuchly, "Modeling of antennas for mobile communication," in *Proc. 12th International Conference on Microwaves and Radar*, (MIKON'98) Warsaw, Poland, vol. 2, pp. 289-293, 1998.

[13] S. Caorsi and A. Massa, "A microwave-imaging technique for electromagnetic exposure prediction: Preliminary results," *Microwave Opt. Technol. Lett.*, vol. 19, no. 5, pp. 328-332, 1998.

[14] S. Caorsi and A. Massa, "Electromagnetic field prediction inside biological bodies by using an inverse scattering procedure based on a statistical cooling algorithm," *Bioelectromagnetics*, vol. 21, no.6, pp. 422-431, 2000.

[15] O. Bucci, G. D'Elia, and D. Migliore, "An effective near-field far-field transformation technique from truncated and inaccurate amplitude-only data," *IEEE Trans. Antennas Propagat.*, vol. 47, no. 9, pp. 1377-1385, 1999.

[16] O. Bucci, A. Capozzoli, and G. D'Elia, "Diagnosis of array faults from far-field amplitude-only data," *IEEE Trans. Antennas Propagat.*, vol. 48, no. 5, pp. 647-652, 2000.

[17] Y. Ramhat-Samii and R. G. Yaccarino, "Microwave antenna imaging, diagnostic and phaseless reconstruction," *Int. J. Imaging Syst. Tech.*, vol. 8, no.4, pp. 396-406, 1997.

[18] R. G. Yaccarino and Y. Rahmat-Samii, "Phaseless bi-polar planar near-field measurements and diagnostics of array antennas," *IEEE Trans. Antennas Propagat.*, vol. 47, no. 3, pp. 574-583, 1999.

[19] R. Pierri, G. D'Elia, and F. Soldovieri, "A two probes scanning phaseless near-field far-field transformation technique," *IEEE Trans. Antennas Propagat.*, vol. 47, pp.792-802, 1999.

[20] E. Polak, *Computational Methods in Optimization*. New York: Academic Press, 1971.

[21] D. S. Jones, *The Theory of Electromagnetism*. Oxford: Pergamon Press, 1964.

[22] J. H. Richmond, "Scattering by a dielectric cylinder of arbitrary cross-section shape," *IEEE Trans. Antennas Propagat.*, vol. 13, pp. 334-341, 1965.

[23] S. Kirkpatrick, C. D. Gelatt, and M. P. Vecchi, "Optimization by simulated annealing," *Science*, vol. 220, pp. 671-680, 1983.

[24] L. Garnero, A. Franchois, J. P. Hugonin, C. Pichot, and N. Joachimowitz, "Microwave imaging - Complex permittivity reconstruction by simulated annealing," *IEEE Trans. Microwave Theory Tech.*, vol. 39, no. 11, pp. 1801-1807, 1991.

[25] S. Caorsi, G. L. Gragnani, S. Medicina, M. Pastorino, and G. Zunino, "Microwave imaging method using a simulated annealing approach," *IEEE Microwave Guided Wave Lett.*, vol. 1, no. 11, 1991.

[26] S. Caorsi, A. Massa, and M. Pastorino, "Optimization procedure based on a statistical cooling method applied to scattering by bounded nonlinear objects," *Radio Sci.*, vol. 31, no. 2, pp. 437-450, 1996.

[27] B. Hajek, "Cooling schedules for optimal annealing," *Math. of Op. Research*, vol. 13, pp. 311-329, 1988.

[28] A. C. Balanis, *Advanced Engineering Electromagnetics*. New York: Wiley, 1989.

[29] IROE, "Dielectric properties of body tissues," Internet Resource, *http://safeemf.iroe.fi.cnr.it/tissprop*